References and Notes

1. C. Sagan, *Icarus* **15**, 511 (1971).
2. W. K. Hartmann, *J. Geophys. Res.*, in press; compare with C. Chapman, J. B. Pollack, C. Sagan, *Astron. J.* **74**, 1039 (1969).
3. C. Sagan, *J. Geophys. Res.*, in press; C. Sagan *et al.*, *ibid.*, in press.
4. W. M. Sinton, *Icarus* **6**, 222 (1967); R. Beer, R. H. Norton, J. V. Martonchik, *ibid.* **15**, 1 (1971).
5. J. Houck, J. B. Pollack, C. Sagan, D. Schaack, J. A. Decker, *ibid.* **18**, 470 (1973).
6. C. Sagan, J. Phaneuf, M. Ihnat, *ibid.* **4**, 43 (1965); see also A. Binder and D. P. Cruikshank, *ibid.* **5**, 522 (1966).
7. G. R. Hunt, L. M. Logan, J. W. Salisbury, *ibid.* **18**, 459 (1973).
8. B. Conrath *et al.*, *J. Geophys. Res.*, in press.
9. R. P. Sharp, L. A. Soderblom, B. C. Murray, J. A. Cutts, *ibid.* **76**, 331 (1971); D. Belcher, J. Veverka, C. Sagan, *Icarus* **15**, 241 (1971).
10. L. A. Soderblom, T. J. Kriedler, H. Masursky, *J. Geophys. Res.*, in press.
11. Liquid CO_2 as the excavating material requires implausibly large quantities of CO_2 to be today sequestered on Mars: CO_2 cannot escape from the planet. High-velocity streams of fluidized sand may exist on Mars, but the surface markers of high-speed winds do not correspond with the distribution of channels (*3*), and braided channels remain mysterious in this hypothesis.
12. R. B. Leighton and B. C. Murray, *Science* **153**, 136 (1966).
13. P. Gierasch and O. B. Toon, *J. Atmos. Sci.*, in press.
14. B. C. Murray, L. A. Soderblom, J. A. Cutts, R. P. Sharp, D. J. Milton, R. B. Leighton, *Icarus* **17**, 328 (1972).
15. B. C. Murray, M. C. Malin, S. C. Yeung, preprint.
16. The large martian volcanoes have volumes of the order of 10^{21} cm^3. Since the entire observable volume of such a volcano must be melted during its formation, and since we know (*5*) that $\sim$ 1 percent by mass of the martian surface material is water of crystallization (a typical value for terrestrial minerals as well), $\sim 10^{19}$ g of water vapor must have been released in the formation of each volcano. The concentration ratio $[CO_2]/[H_2O]$ for Mars is uncertain. Counting the oceans and the carbonates in the sedimentary column, it is $\sim$ 1/6 for the earth. In the atmosphere of Venus this ratio is $> 10^3$. Atmospheric abundances can be dominated by the vapor pressure curve of water. If we adopt $[CO_2]/[H_2O] \sim 1$ for the martian surface, then the evolution of a single large shield volcano releases over the whole surface of Mars $CO_2 \sim 10$ g cm^{-2} from the substance of the volcano itself. Allowing for gases vented from the martian interior; for the existence of several large shield volcanoes, many smaller ones, and the remnants of highly eroded ancient volcanoes (M. Carr, *J. Geophys. Res.*, in press); and for the great uplifted plateaus and ridges on which the volcanoes sit, a total outgassing over the history of Mars of $\gtrsim$ 1 bar of CO_2 does not appear implausible. Nitrogen has not been identified in the martian atmosphere, but this is not a good argument against extensive outgassing on Mars. In the absence of contemporary microbiological activity, most of the nitrogen in the earth's atmosphere would be present as nitrates in the crust.
17. C. Sagan, Technical Report TR 32-34, Jet Propulsion Laboratory, Pasadena, California (1960); A. P. Ingersoll, *J. Atmos. Sci.* **26**, 1191 (1969); S. I. Rasool and C. deBerg, *Nature* **226**, 1037 (1970); J. B. Pollack, *Icarus* **14**, 295 (1971); C. Sagan and G. Mullen, *Science* **177**, 52 (1972).
18. B. C. Murray, W. R. Ward, S. C. Yeung, *Science* **180**, 638 (1973).
19. See, for example, H. H. Lamb, *Climate: Present, Past, and Future* (Methuen, London, 1972).
20. W. R. Ward, *Science* **181**, 260 (1973).
21. D. Ezer and A. G. W. Cameron, *Nature Phys. Sci.* **240**, 180 (1972); F. W. W. Dilke and D. O. Gough, *Nature* **240**, 262 (1972); R. T. Rood, *Nature Phys. Sci.* **240**, 178 (1972); ———, W. A. Fowler, F. Hoyle, *Bull. Amer. Astron. Soc.*, in press.
22. C. Sagan and A. T. Young, *Nature* **243**, 459 (1973).
23. See, for example, G. S. Golitsyn, *Icarus* **18**, 113 (1973); G. Briggs, in preparation; P. Gierasch and R. M. Goody, *J. Atmos. Sci.*, in press.
24. C. Sagan, *The Cosmic Connection* (Doubleday, New York, in press); *Icarus*, in press; see also J. Burns and M. O. Harwit, *ibid.* **19**, 126 (1973).
25. C. Leovy and Y. Mintz, *J. Atmos. Sci.* **26**, 1167 (1969).

26. We are grateful to the members of the Mariner 9 scientific and engineering teams, and to our Mariner 9 colleagues with whom we have discussed the channels, particularly Bruce Murray, Harold Masursky, Daniel Milton, John McCauley, Paul Fox, and Joseph Veverka. We are indebted to Paul Fox for the compilation, to be published elsewhere, on which Fig. 2 is based. Supported in part by NASA grant NGR 33-010-082 and NASA/JPL contract 952487.

4 May 1973; revised 23 July 1973 ■

Montmorillonite: Electron-Optical Observations

Abstract. *Fine-grained micas are consistent impurities in Camp-Berteaux (Morocco) and Wyoming montmorillonites. These micas give selected-area electron diffraction spot patterns with triclinic, monoclinic, and hexagonal symmetries similar to those reported previously for montmorillonites. Camp-Berteaux montmorillonite appears as folded and flexible polycrystalline aggregates with pronounced texturing along the [02], [11], and [1$\bar{1}$] directions. Wyoming montmorillonite displays better crystallinity and larger crystallite size, and its structure is no longer truly "turbostratic."*

Montmorillonite is the principal mineral in bentonites, and therefore it is the most common smectite in nature. Because of its unusual physical properties, this mineral has a wide range of technical applications in fluids used in drilling oil wells, in the ferrous metal industry, in paper and pharmaceutical products, and so forth. These unusual properties of the mineral are related to its crystal structure, morphology, and particle size. A combination of a transmission electron image with a selected area electron diffraction (SAD) pattern provides probably the most effective means for studying the structure and morphology of this mineral. Extensive investigations along this line were carried out by Mering and Oberlin (*1*), who made excellent contributions to our understanding of this subject. They believed that they had obtained SAD patterns from single montmorillonite layers. Recently, SAD patterns were also published for single montmorillonite layers by Roberson and Towe (*2*). The investigators mentioned above, however, had no micrographs of the single montmorillonite layers giving rise to these diffraction patterns.

The symmetry determinations on montmorillonite single crystals by various investigators were not quite in agreement, although samples from the same type localities were studied. Specifically, Mering and Oberlin (*1*) proposed the space group $C2$ for the Wyoming montmorillonite, whereas others suggested triclinic (*2*) and hexagonal (*3*) symmetry for it. A similar situation exists for the Camp-Berteaux montmorillonite from Morocco.

I have carried out extensive electron-optical investigations on a large number of bentonites (*4*). Some of the results, which are summarized in this report, may provide an explanation for the discrepancy between the reports of other investigators. Observations on montmorillonites from two type localities, Camp-Berteaux and Wyoming, are discussed here.

The fractions of the samples less than 2 μm in equivalent spherical diameter were separated by centrifugation

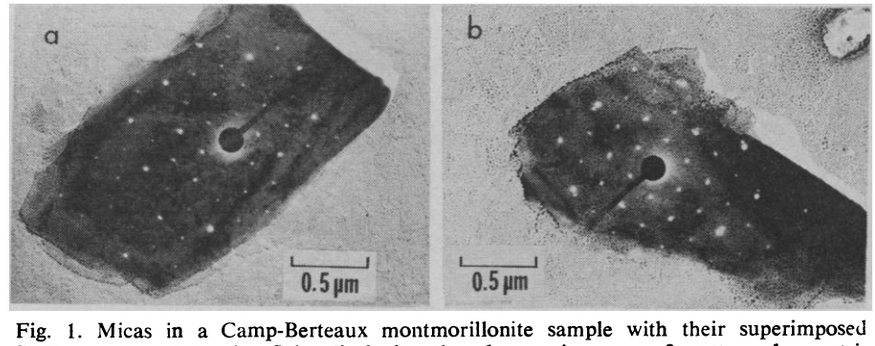

Fig. 1. Micas in a Camp-Berteaux montmorillonite sample with their superimposed SAD patterns: (a) mica flake displaying the plane point group 2 pattern, hence triclinic symmetry; (b) mica flake displaying hexagonal symmetry.

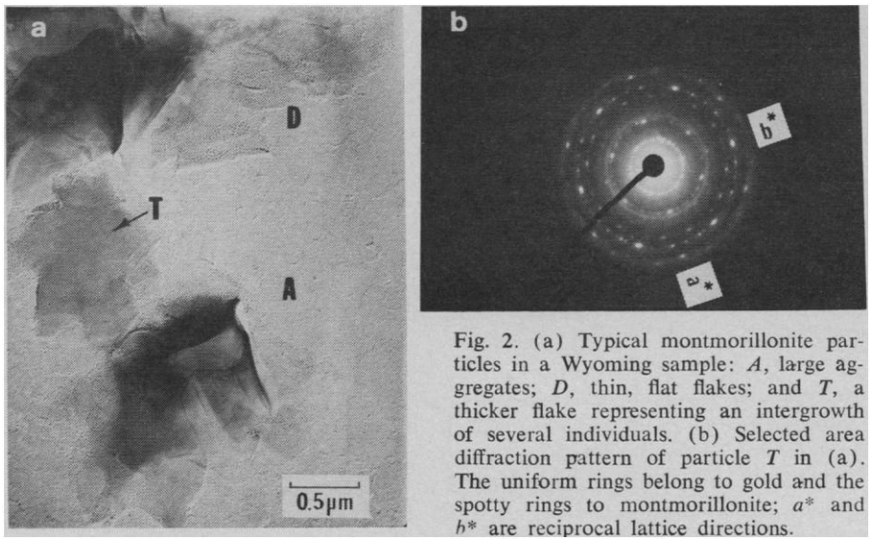

Fig. 2. (a) Typical montmorillonite particles in a Wyoming sample: *A*, large aggregates; *D*, thin, flat flakes; and *T*, a thicker flake representing an intergrowth of several individuals. (b) Selected area diffraction pattern of particle *T* in (a). The uniform rings belong to gold and the spotty rings to montmorillonite; a^* and b^* are reciprocal lattice directions.

and a drop of the suspension so obtained was diluted to a concentration of a few parts per million in a mixture (700 : 1) of distilled water and tertiary butylamine (*5*). A drop of this dilute suspension was dried on a Formvar film and the grid was coated with gold at a shadowing angle of about 26°. This angle provides a simple 2 : 1 ratio between the length of the shadow and the thickness of the particle. Shadowing with gold gives an excellent contrast to electron images so that very thin flakes may be identified by their white rims. Otherwise, these particles are practically invisible and one cannot see the flake giving rise to the diffraction pattern. Samples were also saturated with sodium in case the mineral was not a sodium clay in its natural state. A JEM-7 electron microscope (Japan Electron Optics Laboratory Co.), equipped with a completely variable field-limiting aperture, was operated at 80 kv and the following observations were made.

In the fraction of the Camp-Berteaux montmorillonite smaller than 2 μm there are minor amounts of mica flakes which escape observation by x-ray diffraction. But these micas frequently come under the electron beam and SAD then gives excellent spot patterns. Such a mica flake, with the SAD pattern superimposed on the image, is shown in Fig. 1a. The SAD pattern has strictly the symmetry of plane point group 2, indicating a triclinic symmetry with the possible space groups $C\bar{1}$ or $C1$. A similar SAD pattern was published by Roberson and Towe (*2*) for Camp-Berteaux montmorillonite. They assumed, however, that the fine fraction of the sample was pure montmorillonite and, therefore, assigned the diffraction pattern to a single montmorillonite layer. Since they were working strictly in the diffraction mode, they were not able to see the images of the particles giving rise to the diffraction pattern. Another mica flake in the same sample displays hexagonal symmetry with the plane point group *6mm*, or very close to it (Fig. 1b). Similar micas are also present in much smaller sizes and in thinner flakes. Some of them display the point group *2mm* in SAD patterns, indicating a monoclinic symmetry.

Typically, montmorillonite flakes in the Camp-Berteaux sample seem to be rather irregular, flexible aggregates with folds and curled edges. For thin montmorillonite flakes the *hk* diffraction rings are broken into a series of arcs indicating pronounced texture along the [11], [02], and [$1\bar{1}$] directions. These patterns represent polycrystalline aggregates with fine crystallite sizes where the crystallites have preferred azimuthal orientations along the texture directions.

Particles in Wyoming montmorillonite display morphological features that are distinctly different from those of the Camp-Berteaux sample. They have larger dimensions and form rather flat flakes. Irregular folding and curling of the particles are still present, but to a much lesser extent. Figure 2a shows three types of particles: thin, flat ones (*D*), a thicker one (*T*), and two larger folded aggregates (*A*). Selected area diffraction on thin particles (*D*) gives a spotty ring pattern. The thicker montmorillonite particle (*T*) also gives a spotty ring pattern (Fig. 2b), which illustrates some of the complications with SAD on montmorillonite particles. The intensities for a set of spots from an apparent single crystal are much stronger than those for the other spots along the same diffraction ring. There are five distinct spots between the 02 and 11 reflections. Nine such spots are, however, resolved between the 06 and 33 reflections. The formation of distinct spots indicates an increase of crystallite size. Furthermore, the stacking of the elemental layers in each crystallite can no longer be truly turbostratic (*6*). and they may have definite orientations about the direction normal to the layers in a random sequence. The intensity distribution over the main spots of the apparent single crystal has a symmetry close to hexagonal for the 02, 11; 20, 13; and 06, 33 sets of reflections. The 04 reflection has stronger intensity than the 22 and $2\bar{2}$ reflections, which reduces the symmetry of the pattern to monoclinic. A similar SAD pattern obtained by Mering and Oberlin (*1*) was attributed to the presence of a montmorillonite single layer. The electron transmission image of particle *T* (Fig. 2a) giving rise to the SAD pattern in Fig. 2b shows at least three major individual crystallites in a somewhat trigonal arrangement. If these individuals were of equal volumes, the SAD pattern would be exactly hexagonal. Unequal volumes of crystallites or a partial preferred orientation in the stacking sequence of elemental layers within them may result in monoclinic or triclinic symmetry on the SAD pattern. The additional weak spot along the rings may indicate the presence of several other smaller crystallites with random azimuthal orientations. Thus, my interpretations of the electron-optical data on Wyoming montmorillonite do not agree with those of Mering and Oberlin (*1*). I fully account for the discrepancies and question Mering's model for montmorillonite in a more detailed report elsewhere (*7*).

Although Wyoming montmorillonite seems to be a very suitable sample in which to isolate single montmorillonite crystals, I was not able to do so. Whenever I found a single crystal pattern in the diffraction mode, it turned out to be a thin mica when I took a transmission electron image.

Note added in proof: The impurities, which have been identified as micas in this report, may be chlorite or kaolinite in some cases. This is irrelevant to my argument. It is important to realize that these impurities are present and they give the SAD patterns discussed above.

NECIP GÜVEN

Department of Geosciences, Texas Tech University, Lubbock 79409

References and Notes

1. J. Mering and A. Oberlin, *Clays Clay Miner.* **15**, 3 (1967); in *Electron-Optical Investigations of Clays*, J. A. Gard, Ed. (Monograph 3, Mineralogical Society, London, 1971), p. 208.
2. H. E. Roberson and K. M. Towe, *Science* **176**, 908 (1972).
3. J. M. Cowley and A. Goswami, *Acta Crystallogr.* **14**, 1071 (1961).
4. I thank Dr. R. E. Grim of the University of Illinois for the samples of bentonites from his invaluable collection.
5. This mixture has a *p*H of about 11, which considerably reduces aggregation of particles as shown by J. L. McAtee, Jr., and W. Henslee [*Amer. Mineral.* **54**, 869 (1969)].
6. The term "turbostratic" was suggested by J. Biscoe and B. E. Warren [*J. Appl. Phys.* **13**, 370 (1942)] for superposition of layers with a completely random orientation about the layer normal. A turbostratic sequence is then expected to give uniform diffraction rings on the SAD pattern. Stacking of layers with definite orientations (such as multiples of 60° about the layer normal) but with a random sequence will give a spot pattern like that of a single crystal, although the lattice is still two-dimensional. Therefore, the observation of spot pattern with SAD does not necessarily indicate the presence of single montmorillonite layers, as assumed by Roberson and Towe (*2*).
7. N. Güven, *Clays Clay Miner.*, in press.

15 March 1973; revised 16 July 1973

Deep-Sea Species Diversity: Decreased Gastropod Diversity at Abyssal Depths

Abstract. *Gastropod species diversity is low on the continental shelf, high on the continental slope and abyssal rise, and then decreases with increasing distance out onto the abyssal plain. Increased diversity below the continental shelf has been attributed to increased environmental stability. Decreased diversity on the abyss may result from extremely low productivity.*

The continental slope (about 200 to 2000 m in depth) and abyssal rise (about 2000 to 4000 m in depth) are known to support very diverse deep-sea benthic communities (*1*). But there has been no detailed comparative study of macroinvertebrate species diversity on the abyssal plain (below 4000 m), which is the deepest and most extensive benthic region. In this report, benthic gastropod diversity is analyzed for 24 stations situated along the Gay Head (Massachusetts)–Bermuda transect (*2*) from 70 to 4970 m in depth (Fig. 1).

The samples were collected with an epibenthic sled (*3*) except for stations 171 and 173 on the continental shelf, which were sampled with an anchor dredge (*2*). All the samples came from soft oozes similar in particle size (*2*), so that the faunal comparisons made are probably "within habitat" (*4*). The total gastropod sample from the 24 stations comprised 136 species distributed among 9034 individuals. Only specimens taken alive were used in the analysis.

Several methods were used to compare species diversity among the samples. In the first, individual samples were treated by rarefaction methodology (*5*) to reduce sample sizes to a common number of individuals, and then the Shannon-Wiener information function was applied to the rarefied samples. The information function is expressed as

$$H' = -\sum_{i=1}^{s} p_i \log p_i$$

where p_i is the proportion of species i and s is the number of species in a sample. The function H' is influenced by both the number of species in the sample and the evenness of their distribution among the individuals in the sample. Evenness was measured as $J' = H'/H_{max}$, where $H_{max} = \log s$ is the maximum value of H', which occurs when all species in the sample are equally distributed among the individuals (*6*).

The spectrum of diversity with increasing depth among the 24 samples, all rarefied to 68 individuals, is presented in Fig. 2. (Sixty-eight individuals was the smallest number that included all of the sample sizes.) The pattern of diversity depicted in Fig. 2 obtains for all rarefied sample sizes between 68 individuals and the total sample size. H' at 68 individuals is correlated with

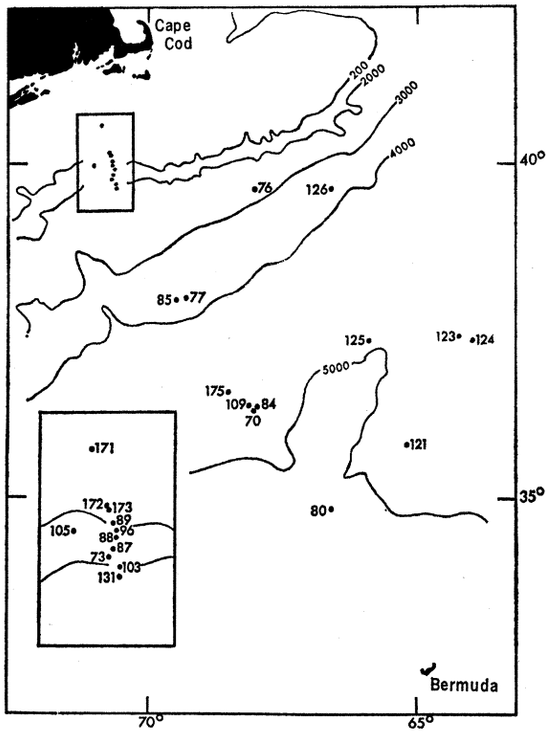

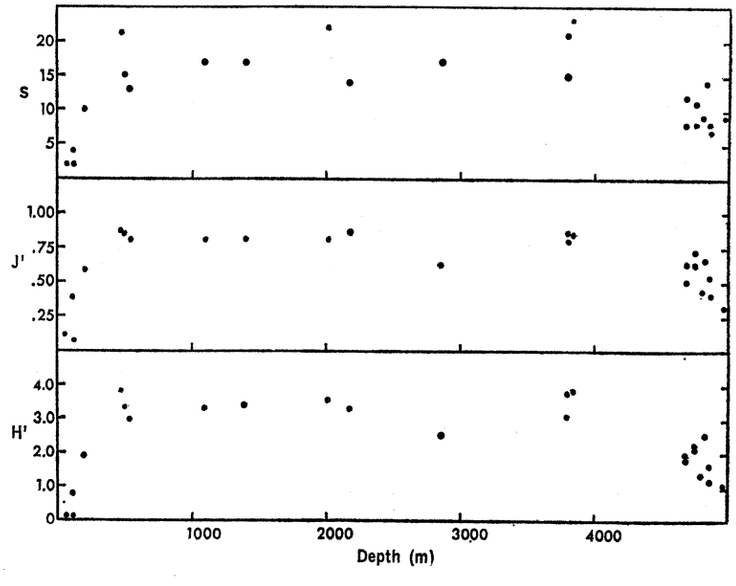

Fig. 1 (left). Localities of samples analyzed in this study. The numbers refer to Woods Hole Oceanographic Institution benthic stations. Fig. 2 (right). Spectrum of gastropod species diversity with increasing depth along the Gay Head–Bermuda transect. H', Shannon-Wiener information function; J', Pielou's measure of species evenness; and s, number of species. All samples have been rarefied to 68 individuals.